Int. J. Electrochem. Sci., 17 **(2022)** Article Number: 220330, doi: 10.20964/2022.03.28

International Journal of
ELECTROCHEMICAL
SCIENCE
www.electrochemsci.org

Short Communication

Preparation of N-doped TiO_2/Biochar Composite Catalysts and its Application for Photoelectrochemical Degradation of Cephalosporin Antibiotics

Huaisheng Hu

College of Chemistry & Chemical Engineering, Longdong University, Qingyang 745000, China
E-mail: huaishenghuh@163.com

Received: 13 November 2021 / *Accepted:* 6 January 2022 / *Published:* 2 February 2022

Many researchers are interested in using TiO_2 semiconductor photocatalysts to combat pollution and solve energy shortages. This study proposes a composite of TiO_2 and biochar because TiO_2 can only use 43 percent of the visible light from sunlight. Meanwhile, nitrogen doping has been used to improve the N-doped TiO_2/biochar composite. The N-doped TiO_2/biochar can improve the photocatalyst's spectral responsiveness and narrow the forbidden band width. This increases the photocatalyst's ability to absorb visible light. This study compared three different modalities of cephalosporin antibiotic removal with N-doped TiO_2/biochar: electrocatalysis, photocatalysis, and photo-electro-chemical catalysis. Photo-electro-chemical catalysis was found to be far superior to single electrocatalysis and photocatalysis.

Keywords: Photoelectrocatalysis; Cephalosporin; Degradation; Biochar; TiO_2

1. INTRODUCTION

Antibiotic production and use has increased dramatically in the twenty-first century, thanks to accelerating industrialization, rising living standards, and the rapid development of the medical and health-care industries. Despite the fact that antibiotics play an important role in human life, health, and medical progress, 80–90% of antibiotics are discharged in their raw molecular form into the wastewater system [1–4]. Because all wastewater treatment technologies rely on conventional biotechnology, which is only marginally effective at degrading antibiotics with bacterial inhibitory effects, a wide range of resistance genes have been discovered in natural water bodies' bacterial communities. Furthermore, many studies have shown that the coexistence of drugs or other chemicals can cause organisms to develop more complex toxicity [5–8]. Diclofenac, ibuprofen, naproxen, and acipenser monophosphate, for example, can have toxic synergistic effects [9–12]. These circumstances have prompted questions

about the effectiveness of antibiotic removal from the environment and the safety of drinking water, reclaimed water, recycled water, and aquatic ecosystems.

Antibiotics are not effectively removed by conventional wastewater treatments. Antibiotics' long-term presence and transport in the environment pose a risk to aquatic organisms and human life. Antibiotics are also morphologically stable in nature and react with other organic matter in wastewater to produce and transform more complex by-products [13–17]. To avoid surface water contamination and the production of more toxic by-products, antibiotics must be treated before being released into natural water bodies. Cephalosporin antibiotics are the most widely used human and veterinary antibiotics in most countries, accounting for roughly 50–70% of total human antibiotic use. In conventional physical and biological treatment processes, the removal of cephalosporin antibiotics is insufficient [18–21]. Secondary pollution may occur because the traditional adsorption and membrane treatment process for antibiotics is only a simple transfer and cannot be completely degraded or even mineralized. Fenton oxidation technology and sulfate radical oxidation technology are two new advanced oxidation technologies that have only recently begun to be developed and show promising oxidation capabilities [22]. Adding catalytic agents like H_2O_2, Fe^{2+}, and $S_2O_8^{2-}$, on the other hand, increased the difficulty and cost of subsequent treatment.

In recent years, electrocatalytic oxidation technology has gotten a lot of attention and has seen rapid development in the scientific community. Electrocatalytic oxidation technology can rapidly oxidize organic matter into low or non-toxic products, and even completely mineralize difficult-to-degrade organic matter, thanks to its advantages of simple equipment, strong oxidation, large treatment capacity, safety and reliability, and no need for additives [23–26]. Catalytic oxidation is a highly manipulable technology that can easily be combined with other water treatment methods. The electrochemical system's modular design and small footprint also make it ideal for decentralized wastewater treatment [27]. Semiconductor photocatalysis, a type of advanced oxidation method, is a popular research topic in wastewater treatment, with obvious benefits for difficult-to-degrade organic waste. Photocatalysis is a photocatalytic technique in which photogenerated electrons are moved to an external circuit by an applied voltage, speeding up the separation of electrons and holes [28–30]. Photocatalysis technology has gotten a lot of attention and research in recent years because of its ability to generate hydrogen and reduce hydrocarbon dyes while degrading organic pollutants using solar energy.

Because of its advantages of high catalytic efficiency, environmental friendliness, and good stability, TiO_2 has attracted a lot of attention as one of the most widely and intensively researched systems in the field of photocatalysis so far [31,32]. However, acute anatase TiO_2 can only absorb 4% of ultraviolet light from sunlight and cannot absorb 43% of visible light, limiting its potential for practical applications. Many efforts have been made by researchers to broaden the response to visible light, including doping of metallic and non-metallic elements, as well as mixed metal doping [33]. Despite their good response to visible light, the disadvantages of easy recombination of photogenerated electron-hole pairs, poor stability, and the high cost of metals prevent them from being widely used in practice [34].

Under anaerobic or anoxic conditions [35,36], biochar is a carbon material produced by the high-temperature pyrolysis of agricultural and forestry waste such as rice husks, straw, bagasse, and other

environmental organisms. Biochar has attracted more attention because of its rich variety of functional groups on the surface, its developed pore structure, good chemical stability, and its large surface area [37]. Currently, there are many reports on the composite of carbon nanotubes, graphene, and activated carbon with TiO_2 semiconductor materials to enhance photocatalytic activity. However, these materials are not easy to prepare, the conditions are strict, the cost is relatively high, and mass production is not practical. Biochar is suitable for forming composites with TiO_2 because of its simple preparation method, low preparation cost, and good electron migration ability. Therefore, biochar compounded with TiO_2 and modified with nitrogen doping is of high research value as a possible photoelectrochemical catalytic material to improve the efficacy of wastewater treatment.

2. EXPERIMENTAL

2.1 Preparation of biochar, biochar/TiO_2 composite and N doped biochar/TiO_2 composite

Wheat straw was used as the starting material for making biochar. Wheat straw was washed and dried after being washed with water to remove dust and soil. Crush wheat straw with a pulverizer and pass it through a 100 mesh sieve. The above-prepared wheat straw powder was weighed and placed in a crucible, which was then sealed with high purity nitrogen and reacted for 2 h at a specific calcination temperature (heating rate of 5°C/min) in a box-type muffle furnace, yielding biochar (denoted as BC).

In a conical flask, drop 10 mL of butyl titanate into 30 mL of anhydrous ethanol and stir until the solution is well mixed. Solution A should be labeled. In the prepared pear-shaped funnel, combine 10 mL anhydrous ethanol, 1 mL water, and 1 mL acetic acid. Solution B has been labeled. Add solution B to solution A drop by drop, stir for 30 minutes to get a white solute, and store in the dark for 24 h. To the conical flask, add 0.01 g of BC and various amounts of solute, and stir for 30 minutes. In a conical flask, combine 0.01g BC and various amounts of sol, stir for 30 minutes, add a small amount of water to further hydrolyze the sol, and finally add biochar to make the entire sol lose its fluidity. The conical flask was placed in an oven at 80°C for several hours and finally turned into a black solid mass. The black solid was ground into powder and heated in a muffle furnace for 2 h at 500°C under nitrogen protection. Biochar/TiO_2 composite (abbreviated BC/TiO_2) was created. In order to make the N-doped biochar/TiO_2 composite, a small amount of urea was added to the B solution preparation.

Hot pressing was used to make the electrode. Ultrasonic treatment for 30 minutes after weighing 0.5 g of the above powder into a 100 mL beaker, adding a certain amount of ethanol, and 0.l mL of PTFE solution. In the oven, the solvent evaporated and formed a gel. Under 20 MPa pressure, the electrode was pressed into a stable sheet electrode, washed with water, and dried in an oven at 80°C for 2 hours.

2.2 Photoelectrochemical catalytic degradation of cephalosporin antibiotics

Weigh 200 mg of cephalosporin antibiotic dissolved in water and fix the volume to 1000 mL with a volumetric flask. The cephalosporin solution, which had been prepared in 200 mL, was diluted to the desired concentration gradient. A magnetic stirrer was used to stir 150 mL of cephalosporin solution, and sodium sulfate solid was added as a supporting electrolyte. All reactions were carried out in a glass

apparatus with a photocatalytic light source of a xenon lamp (150 W). Working electrodes were made from hot pressed electrodes, and the cathode was made from titanium sheet. The distance between the two electrodes was kept to a minimum of two centimeters. Before the reaction, the solution was stirred in the dark to achieve the adsorption-desorption equilibrium. The light source was then turned on to carry out the corresponding catalytic reactions, and the applied voltage was controlled by the applied power supply. The catalytic reactions were carried out under electrocatalysis, photocatalysis, and photo-electrocatalysis conditions, respectively.

3. RESULTS AND DISCUSSION

The XRD spectra of BC, pure TiO_2, BC/TiO_2, and N-doped TiO_2/biochar are shown in Figure 1. BC has diffraction peaks at 2=26.6° and 2=45°, which correspond to the carbon structure (002) and (100) planes, respectively (JCPDS 01-0640). Pure TiO_2 has diffraction peaks at 25.3 degrees (101), 38.1 degrees (004), 48.2 degrees (200), 54.1 degrees (105), 54.9 degrees (211), 62.8 degrees (204), and 69.3 degrees (220), indicating that TiO_2-500 is an anatase crystal type (JCPDS 21-1272). The carbon structure (002) and (100) facets (JCPDS 01-0640) correspond to the diffraction peaks of BC at 2=26.6° and 2=45° [38]. The diffraction peaks of BC/TiO_2 composites are nearly identical to those of pure TiO_2, demonstrating that the addition of BC has no effect on TiO_2's crystalline form. The crystallographic planes (101), (004), (200), (105), (211), (204), and (220) of the anatase type of TiO_2 correspond to the diffraction peaks of N-doped TiO_2/biochar at 2=25.3°, 38.1°, 48.2°, 54.1°, 54.9°, 62.8°, and 69.3°, indicating that nitrogen doping does not change the crystallographic shape of TiO_2 [39]. The intensity of the composite's diffraction peak (101) is weakened, and the (302) crystal plane of $TiO_{0.34}N_{0.74}$ appears at 2=32.2° for N-doped TiO_2/biochar (JCPDS 44-0951), indicating that nitrogen doping enters the TiO_2 lattice and forms the N-Ti-O structure, which replaces the original O-Ti-O structure [40]. Due to the small amount of nitrogen that enters the TiO_2 lattice, the diffraction peak is very weak. UV-vis diffuse reflectance spectroscopy was used to determine the optical properties of the samples, and the UV-vis spectra of various samples are shown in Figure 2. Pure TiO_2 is insensitive to visible light and does not absorb visible light, as can be seen. The BC/TiO_2 composite has absorption in the visible region with a red-shifted band gap edge after compounding with BC, indicating that compounding BC with TiO_2 can improve TiO_2 absorption in the visible region [41]. The BC has a high capacity for electron migration, which aids in the separation of photogenerated electrons and holes. This increases light absorption and improves the efficiency of visible light utilization [41].

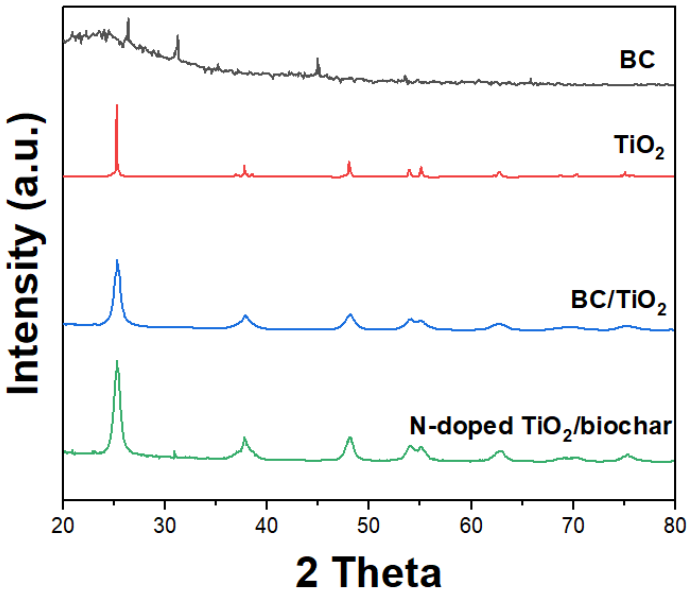

Figure 1. XRD patterns of BC, TiO_2, BC/TiO_2 and N-doped TiO_2/biochar powder.

As a result, the composites' spectral responsiveness has been improved to some extent. The presence of photosensitive functional groups on the BC surface, on the other hand, improves the photocatalytic activity of the composites by increasing light absorption. N-doped TiO_2/biochar absorption in the UV and visible regions was improved even more.

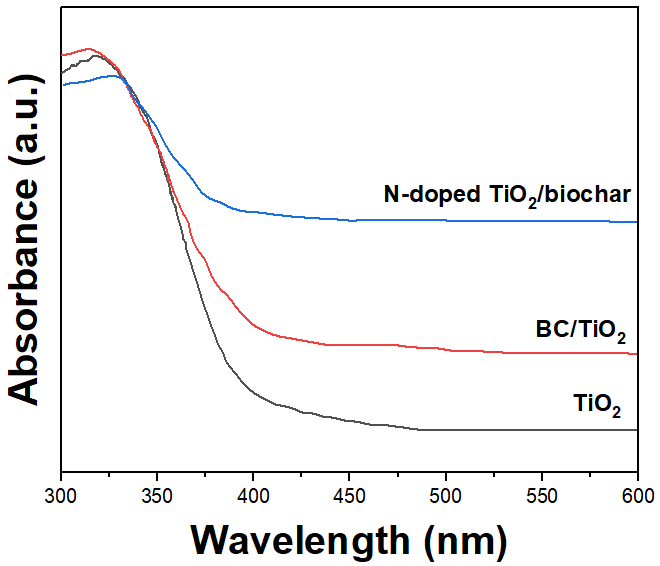

Figure 2. UV-vis spectra of TiO_2, BC/TiO_2 and N-doped TiO_2/biochar powder.

When too much nitrogen is doped into the TiO_2 lattice, it causes the formation of a complex center of photogenerated electrons and holes, which accelerates their complexation rate and makes it impossible to fully utilize the absorbed photon energy at low frequencies, lowering photocatalytic

efficiency [42]. The absorption band edge in the visible region of the N-doped TiO_2/biochar is significantly redshifted, indicating that nitrogen doping narrows the composites' forbidden band width. This increases the use of visible light and broadens the photoresponse range. Simultaneously, the composite can excite more photogenerated carriers per unit time, improving the composite's photocatalytic performance. The ability of nitrogen doping to form heteroenergy levels in the band gap of TiO_2 and the hybridization of N_{2p} with O_{2p} to generate new energy levels can be attributed to the composites' lower band gap energy [43]. SEM images of BC/TiO_2 and N-doped TiO_2/biochar are shown in Figure 3. BC/TiO_2 and N-doped TiO_2/biochar have nearly identical morphologies.

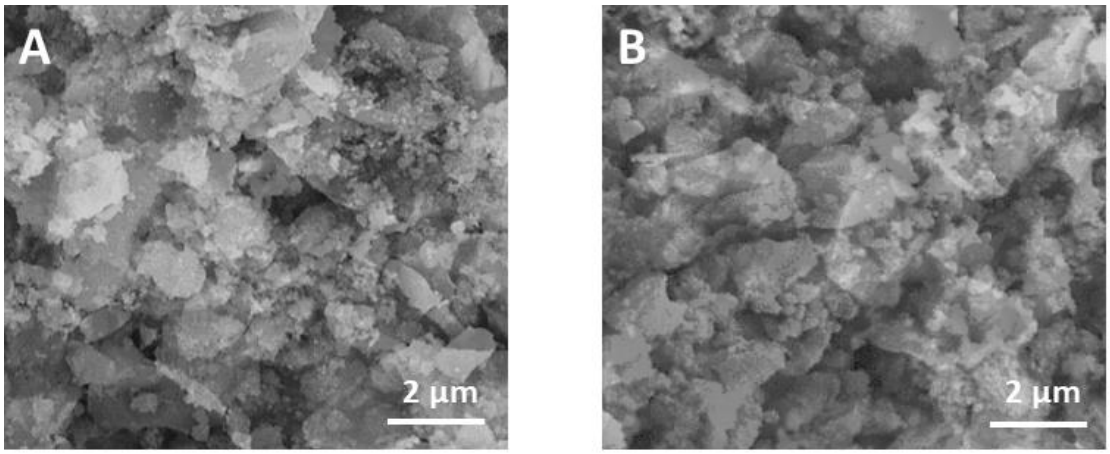

Figure 3. SEM images of (A) BC/TiO_2 and (B) N-doped TiO_2/biochar powder.

The electron leap between the band gaps of TiO_2 semiconductor materials is subject to relaxation and complexation phenomena, so TiO_2 can only absorb a portion of the photons to generate photocurrents. As a result, I-V curves can be used to investigate different samples' photochemical properties (Figure 4A). The photocurrent densities of BC/TiO_2 and N-doped TiO_2/biochar were larger than TiO_2 at various voltages, as shown in the figure [44]. This suggests that the BC composite is important for increasing photoelectric conversion efficiency. Impedance spectroscopy was used to look into the samples' photoelectrochemical properties further (Figure 4B). In both light and dark states, the impedance profiles of TiO_2, BC/TiO_2, and N-doped TiO_2/biochar are shown. Under Xe lamp illumination, the arc radii of TiO_2, BC/TiO_2, and N-doped TiO_2/biochar impedances were all significantly reduced compared to the dark state [45]. This means that when the sample surface was exposed to light, a large number of photogenerated carriers were generated, and the reaction between the electrode and the interface was accelerated, resulting in increased current and lower impedance. The separation efficiency of photogenerated electron-hole pairs was discovered to be related to the arc radius on the impedance diagram. Under light illumination, the arc radius of N-doped TiO_2/biochar is smaller than that of BC/TiO_2, indicating that N-doped TiO_2/biochar has better electron-hole pair separation than BC/TiO_2, which improves photocatalytic and photoelectrochemical performance [46].

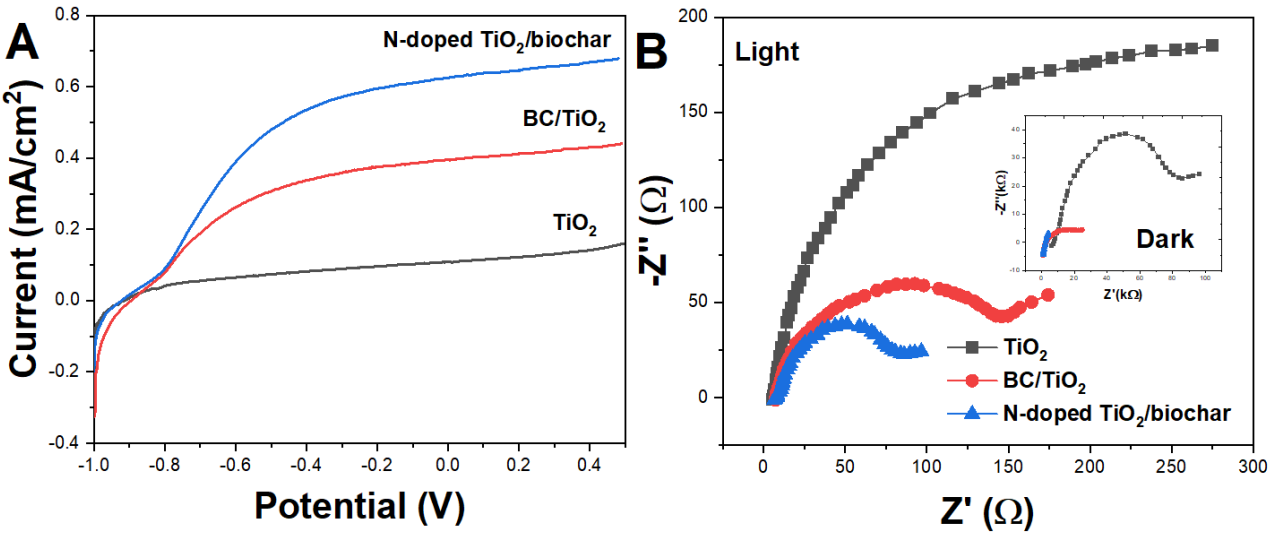

Figure 4. (A) I-V curves and (B) EIS Nyquist plots of TiO_2, BC/TiO_2 and N-doped TiO_2/biochar. Electrolyte: 1 M NaOH; Scan rate (I-V): 10 mV/s; Scan rate: 5 mV/s (EIS).

At a voltage of 0 V, Figure 5 provides a plot of the relationship between time and photocurrent density. As can be seen in the diagram, the sample's current density in the dark condition is near to 0. At the time of illumination, a spike was formed, and the first current was mostly generated by the separation of electron-hole pairs at the sample-electrolyte contact surface [45]. After the spike, the current intensity drops but stabilizes, indicating that some electron-hole pairs have compounded. When the light source is switched off again, the current tends to zero once more. The current density recovers to its previous size when the light is illuminated again, indicating that the prepared sample has strong cycle reversibility.

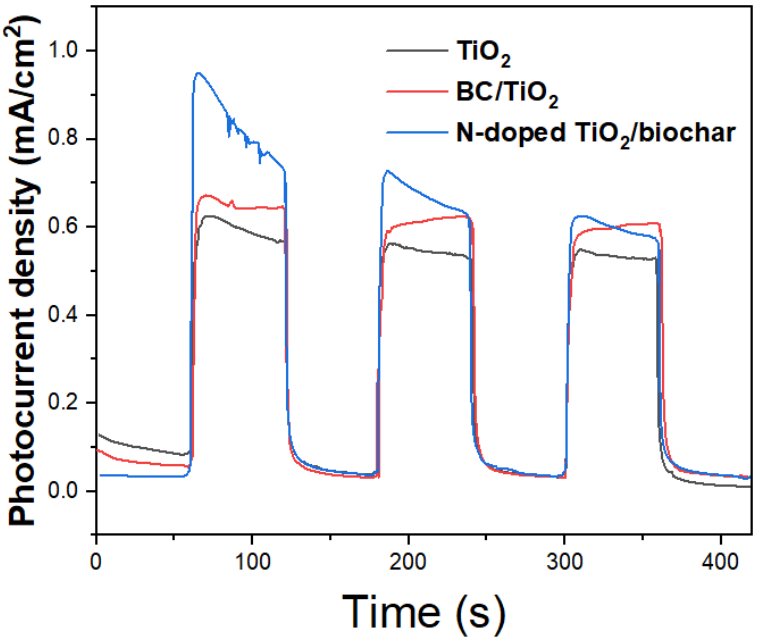

Figure 5. Comparison of transient photocurrent response of BC/TiO_2 and N-doped TiO_2/biochar. Electrolyte: 1 M NaOH.

To examine the photo-electro-chemical performance of N-doped TiO_2/biochar, we first looked at the effects of simple photolysis (without photocatalyst), photocatalysis (UV-visible light), electrocatalysis, and photo-electro-chemical on the elimination of cephalosporin antibiotics (see Figure 6). Under UV-visible light conditions, the removal rates of cephalosporin antibiotics by N-doped TiO_2/biochar after 2 h reaction were 3.5% for photolysis, 20.4% for electrocatalysis, 31.5% for photocatalysis and 91.7% for photo-electro-chemical. It is clear that photo-electro-chemical has a synergistic impact, and the breakdown efficiency of cephalosporin antibiotics is clearly superior to electrocatalysis and photocatalysis alone. A straight line can be obtained by curving ln(C0/C) against time t. Its slope is the apparent rate constant of the photocatalytic reaction. The apparent rate constant k values of the respective reactions are shown in Table 1.

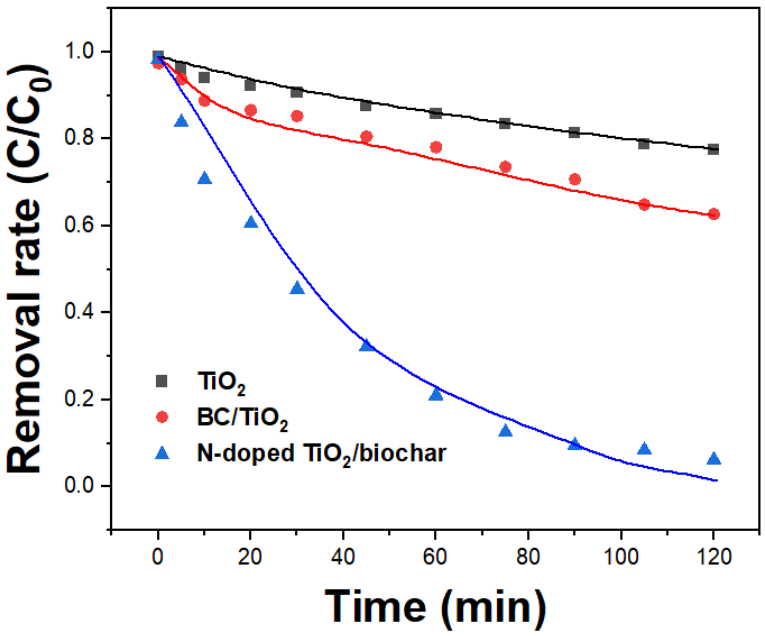

Figure 6. The variation of cephalosporin antibiotics removal vs. time at the N-doped TiO_2/biochar using four different photoctalysts.

Table 1. Values of the apparent rate constant of different condition of cephalosporin antibiotics removal at the N-doped TiO_2/biochar.

Reaction condition	K (min^{-1})	R^2
Photolysis	0.00020	0.957
Electrocatalysis	0.00179	0.981
Photocatalysis	0.00305	0.988
Photoelectrocatalysis	0.02144	0.963

The catalyst's lifetime and consistency of efficiency are other crucial performance parameters that determine its worth in industrial applications. The N-doped TiO_2/biochar electrode was tested for stability and reusability. Figure 7 shows that the performance of N-doped TiO_2/biochar only degrades

slightly after four cycles, indicating that the catalyst's stability and reusability can essentially meet the criteria of continuous operation in industry. Contamination during operation by organic debris or intermediates that adsorb to the catalyst surface and cannot be removed may be the cause of continual degradation of this electrode material.

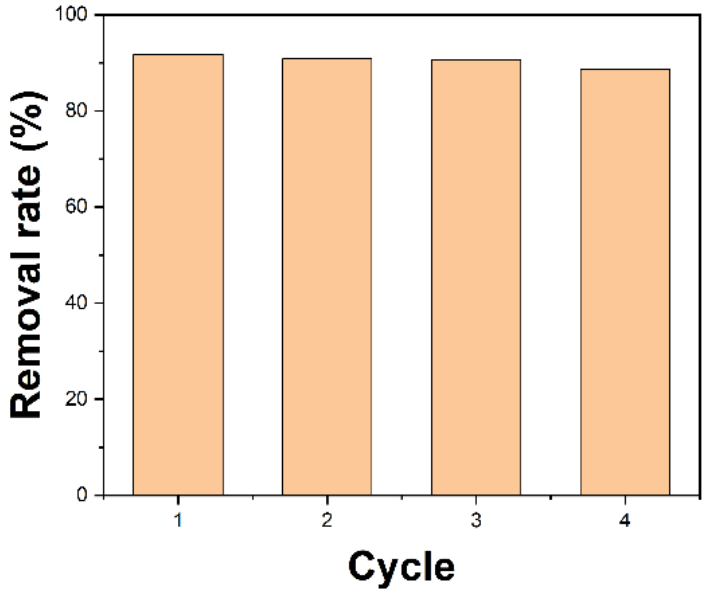

Figure 7. Stability test of N-doped TiO_2/biochar for cephalosporin antibiotics removal for four cycles.

4. CONCLUSION

The sol-gel process was used to make N-doped BC/TiO_2 composites. XRD, UV-vis diffuse reflection, and SEM were used to characterize the composite. Nitrogen doping can significantly improve the specific surface area of composites, allowing for easier organic molecule adsorption. The right amount of N doping allows the electrons in TiO_2 to jump right into the conduction band, and the electron and hole pairs aren't easily compounded, resulting in greater visible photocatalytic performance. This boosts the photocatalyst's absorption of visible light and the utilization of solar energy. The elimination of cephalosporin antibiotics using N-doped TiO_2/biochar was compared using three different modalities of electrocatalysis, photocatalysis, and photo-electro-chemical catalysis. Photo-electro-chemical catalysis was found to be far superior to single electrocatalysis and photocatalysis.

References

1. X. Zhang, H. Zhao, J. Du, Y. Qu, C. Shen, F. Tan, J. Chen and X. Quan, *Environ. Sci. Pollut. Res.*, 24 (2017) 16478.
2. Z. Xu, X. Song, Y. Li, G. Li and W. Luo, *Sci. Total Environ.*, 684 (2019) 23.
3. H. Wen, H. Zhu, B. Yan, Y. Xu and B. Shutes, *Chemosphere*, 250 (2020) 126252.
4. H. Karimi-Maleh, Y. Orooji, F. Karimi, M. Alizadeh, M. Baghayeri, J. Rouhi, S. Tajik, H. Beitollahi, S. Agarwal and V.K. Gupta, *Biosens. Bioelectron.* (2021) 113252.
5. W. Wang, W. Zhang, H. Liang and D. Gao, *Front. Environ. Sci. Eng.*, 13 (2019) 34.

6. J. Wang, L. Chu, L. Wojnárovits and E. Takács, *Sci. Total Environ.* (2020) 140997.
7. J.S. Wallace, E. Garner, A. Pruden and D.S. Aga, *Environ. Pollut.*, 236 (2018) 764.
8. H. Karimi-Maleh, A. Khataee, F. Karimi, M. Baghayeri, L. Fu, J. Rouhi, C. Karaman, O. Karaman and R. Boukherroub, *Chemosphere* (2021) 132928.
9. M.A. Skow, I. Vik and S. Høye, *Infect. Dis.*, 52 (2020) 405.
10. J. Zhou, Y. Zheng, J. Zhang, H. Karimi-Maleh, Y. Xu, Q. Zhou, L. Fu and W. Wu, *Anal. Lett.*, 53 (2020) 2517–2528.
11. L. Fu, J. Zhu and H. Karimi-Maleh, *Biosensors*, 11 (2021), 325.
12. H. Karimi-Maleh, F. Karimi, L. Fu, A.L. Sanati, M. Alizadeh, C. Karaman and Y. Orooji, *J. Hazard. Mater.*, 423 (2022) 127058.
13. J.N. Russell and C.K. Yost, *Chemosphere*, 263 (2021) 128177.
14. A.S. Oberoi, Y. Jia, H. Zhang, S.K. Khanal and H. Lu, *Environ. Sci. Technol.*, 53 (2019) 7234.
15. S. Yan, Y. Yue, L. Zeng, L. Su, M. Hao, W. Zhang and X. Wang, *Front. Chem.*, 9 (2021) 220.
16. H. Karimi-Maleh, A. Ayati, R. Davoodi, B. Tanhaei, F. Karimi, S. Malekmohammadi, Y. Orooji, L. Fu and M. Sillanpää, *J. Clean. Prod.*, 291 (2021) 125880.
17. J. Ying, Y. Zheng, H. Zhang and L. Fu, *Rev. Mex. Ing. Quím.*, 19 (2020) 585.
18. M. Zhang, B. Pan, Y. Wang, X. Du, L. Fu, Y. Zheng, F. Chen, W. Wu, Q. Zhou and S. Ding, *ChemistrySelect*, 5 (2020) 5035.
19. L. Fu, K. Xie, Y. Zheng, L. Zhang and W. Su, *Electronics*, 7 (2018) 15.
20. J. Liu, T. Yang, J. Xu and Y. Sun, *Front. Chem.*, 9 (2021) 488.
21. M. Magureanu, F. Bilea, C. Bradu and D. Hong, *J. Hazard. Mater.* (2021) 125481.
22. H. Karimi-Maleh, M. Alizadeh, Y. Orooji, F. Karimi, M. Baghayeri, J. Rouhi, S. Tajik, H. Beitollahi, S. Agarwal, V.K. Gupta, S. Rajendran, S. Rostamnia, L. Fu, F. Saberi-Movahed and S. Malekmohammadi, *Ind. Eng. Chem. Res.*, 60 (2021) 816.
23. R. Duan, X. Fang and D. Wang, *Front. Chem.*, 9 (2021) 361.
24. L. Fu, Q. Wang, M. Zhang, Y. Zheng, M. Wu, Z. Lan, J. Pu, H. Zhang, F. Chen and W. Su, *Front. Chem.*, 8 (2020) 92.
25. M. Lopez-Carrizales, K.I. Velasco, C. Castillo, A. Flores, M. Magaña, G.A. Martinez-Castanon and F. Martinez-Gutierrez, *Antibiotics*, 7 (2018) 50.
26. A. Holubová, L. Chlupáčová, L. Cetlová, N.A. Cremers and A. Pokorná, *Antibiotics*, 10 (2021) 918.
27. D. Cheng, H.H. Ngo, W. Guo, S.W. Chang, D.D. Nguyen, Y. Liu, X. Shan, L.D. Nghiem and L.N. Nguyen, *Bioresour. Technol.*, 300 (2020) 122707.
28. C. Burrello, F. Garavaglia, F.M. Cribiù, G. Ercoli, S. Bosari, F. Caprioli and F. Facciotti, *Front. Med.*, 5 (2018) 21.
29. E. Bloem, A. Albihn, J. Elving, L. Hermann, L. Lehmann, M. Sarvi, T. Schaaf, J. Schick, E. Turtola and K. Ylivainio, *Sci. Total Environ.*, 607 (2017) 225.
30. R. Yang, B. Fan, S. Wang, L. Li, Y. Li, S. Li, Y. Zheng, L. Fu and C.T. Lin, *Micromachines*, 11 (2020) 967.
31. S. Moles, R. Mosteo, J. Gómez, J. Szpunar, S. Gozzo, J.R. Castillo and M.P. Ormad, *Water*, 12 (2020) 1453.
32. P. Karaolia, I. Michael-Kordatou, E. Hapeshi, C. Drosou, Y. Bertakis, D. Christofilos, G.S. Armatas, L. Sygellou, T. Schwartz and N.P. Xekoukoulotakis, *Appl. Catal. B Environ.*, 224 (2018) 810.
33. T.C.M.V. Do, D.Q. Nguyen, K.T. Nguyen and P.H. Le, *Materials*, 12 (2019) 2434.
34. S. Babić, L. Ćurković, D. Ljubas and M. Čizmić, *Curr. Opin. Green Sustain. Chem.*, 6 (2017) 34.
35. R. Tian, C. Li, S. Xie, F. You, Z. Cao, Z. Xu, G. Yu and Y. Wang, *J. Soils Sediments*, 19 (2019) 2891.
36. C. Li, X. Zhu, H. He, Y. Fang, H. Dong, J. Lü, J. Li and Y. Li, *J. Mol. Liq.*, 274 (2019) 353–

361.
37. D.G. Kim, D. Choi, S. Cheon, S.-O. Ko, S. Kang and S. Oh, *J. Water Process Eng.*, 33 (2020) 101019.
38. Y. Yu, S. Liu, W. Wang, Q. Shang, J. Han, C. Liu, Z. Tian and J. Chen, *Sci. Total Environ.*, 794 (2021) 148688.
39. X. Xie, S. Li, H. Zhang, Z. Wang and H. Huang, *Sci. Total Environ.*, 659 (2019) 529–539.
40. S. Silvestri, M.G. Gonçalves, P.A. da Silva Veiga, T.T. da S. Matos, P. Peralta-Zamora and A.S. Mangrich, *J. Environ. Chem. Eng.*, 7 (2019) 102879.
41. R. Shan, L. Lu, J. Gu, Y. Zhang, H. Yuan, Y. Chen and B. Luo, *Mater. Sci. Semicond. Process.*, 114 (2020) 105088.
42. M.M. Mian and G. Liu, *Chemosphere*, 215 (2019) 101.
43. L. Lu, R. Shan, Y. Shi, S. Wang and H. Yuan, *Chemosphere*, 222 (2019) 391.
44. T. Fazal, A. Razzaq, F. Javed, A. Hafeez, N. Rashid, U.S. Amjad, M.S. Ur Rehman, A. Faisal and F. Rehman, *J. Hazard. Mater.*, 390 (2020) 121623.
45. M. Pinna, G. Binda, M. Altomare, M. Marelli, C. Dossi, D. Monticelli, D. Spanu and S. Recchia, *Catalysts*, 11 (2021) 1048.
46. J.S. Lazarotto, V. de Lima Brombilla, S. Silvestri and E.L. Foletto, *Appl. Organomet. Chem.*, 34 (2020) e6001.